Materials Science & Engineering A 566 (2013) 8–15

Contents lists available at SciVerse ScienceDirect

Materials Science & Engineering A

journal homepage: www.elsevier.com/locate/msea

Development of as-cast dual matrix structure (DMS) ductile iron

S.C. Murcia, M.A. Paniagua, E.A. Ossa *

Engineering Materials Research Group, School of Engineering, Eafit University, Cra 49 No. 7 sur 50, Medellín, Colombia

ARTICLE INFO

Article history:
Received 10 October 2012
Received in revised form
13 December 2012
Accepted 14 December 2012
Available online 28 December 2012

Keywords:
As-cast ductile iron
Dual matrix structure
Martensite
Bainite
Heat treating

ABSTRACT

Ductile iron is widely used due to its low cost and higher ductility than other cast irons. There has been an increased interest during the last years in improving the strength of these materials by means of heat-treating to obtain dual matrix structures (DMS) that enhance the properties found in Austempered Ductile Irons (ADI). This work studies the fabrication of DMS ductile cast irons with martensitic and bainitic structures in the as-cast condition, reducing costs related to heat treating processing while improving the mechanical behavior of the material. Cast irons alloyed with nickel ranging from 0% up to 7% were produced in order to evaluate the effect of Ni–Mo content on the phase transformations and mechanical properties of the material. The effect of cooling rate in phase transformations and mechanical properties were studied using molds with different wall thicknesses, finding that addition of Nickel and Molybdenum improves substantially the strength of the as-cast ductile iron, making unnecessary any further heat treating according to the level of properties desired.

1. Introduction

Ductile iron (DI) is widely used due to its low cost and good mechanical properties, making it an excellent choice for industrial applications as machine parts with medium strength requirements. The Wide range of properties that can be achieved by ductile irons are controlled basically by the shape of the graphite nodules embedded on its metal matrix [1–3]. A number of variables, including chemical composition and cooling rate, can control the matrix structure of ductile iron, and hence its mechanical properties [2,4–9]. In an as-cast state, for a given chemical composition and nodule count, the cooling rate through the austenite transformation range determines the final matrix structure: faster cooling rates promotes pearlite formation, whereas slower cooling rates favor ferrite formation [4]. However, if acicular structures are desired to enhance mechanical properties, heat treatments like quenching, tempering and austempering have to be performed [10–13].

Austempering is one of the most studied heat treatments for DI due to the resulting microstructure consisting of acicular ferrite (α) and high carbon austenite (γ) [14]. Austempered Ductile Iron (ADI) exhibits more than twice the strength for a given level of ductility compared to ductile iron and it can be achieved by a two stages process: in stage I, the austenite matrix with high carbon content isothermally transforms into ausferrite; and in stage II, the stabilized austenite decomposes into ferrite and carbides [15]. In order to achieve optimum mechanical properties, the austempering process needs to be optimized to produce the desired microstructure. Heat treatment parameters such as austempering time and temperature [14,16–21] and austenization kinetics [22,23] have been extensively studied up to the point where the processing window can be determined by numerical modeling [15,24].

Recently, researchers and producers have been focusing their efforts on the development of DI with mixed microstructures or dual matrix structure (DMS): ferritic–bainitic or ferritic–martensitic. These kinds of microstructures make a good combination of mechanical properties and physical characteristics, reaching tensile stresses up to 1.15 GPa with up to 16% of total elongation, depending on the amount of ferrite present in the matrix which ranges from 5% to 85% [1,3,18,19,25–27]. These microstructures are obtained by a special heat treatment process in which the DI is subjected to an incomplete austenitization stage at different temperatures within the intercritical interval, followed by a fast cooling step to transform austenite into ausferrite or martensite (Fig. 1) [1,3,18,19,25–27]. The intercritical interval is a region delimited by the upper and lower critical temperatures, where ferrite, graphite and austenite coexist, as shown in Fig. 2 [3]. Such temperatures define the starting point at which ferrite transforms into austenite and austenite into ferrite in heating and cooling processes, respectively. Ductile iron austemperability can be enhanced by changing the position and amplitude of this interval, which can be done by using alloying elements like copper, nickel and molybdenum, typically added between 0.2% and 5.0% [7,8,15,28–39].

In spite of that, the use of heat treatments implies additional costs to the final product that can be avoided if DMS ductile iron

* Corresponding author. Tel.: +57 4 2619500x9603; fax: +57 4 2664284.
E-mail address: eossa@eafit.edu.co (E.A. Ossa).

0921-5093/$ - see front matter © 2012 Elsevier B.V. All rights reserved.
http://dx.doi.org/10.1016/j.msea.2012.12.033

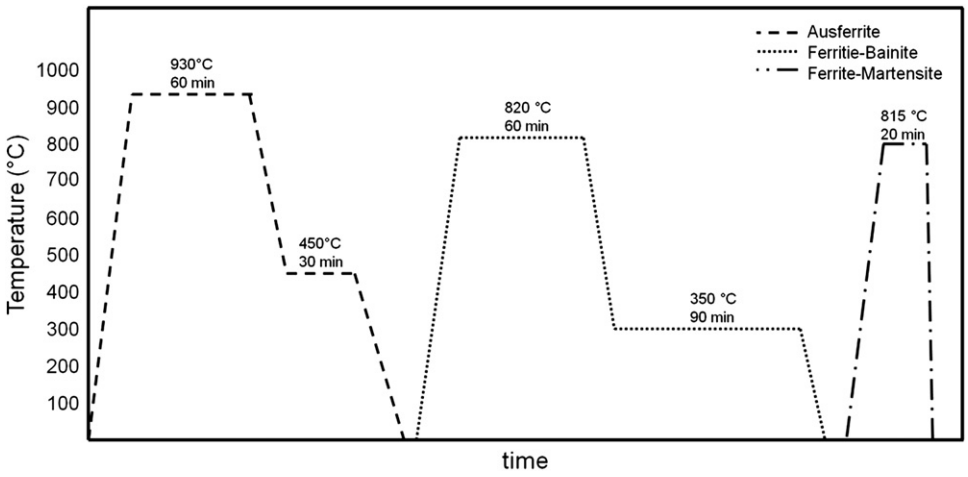

Fig. 1. Schematic representation of heat treatments performed in order to obtain ausferrite, ferrite–bainite and ferrite–martensite microstructures on ductile irons.

is produced directly from the casting process (as-cast). There have been a few studies aiming at producing DMS in an as-cast state, one of the first studies was reported by Flinn et al. [40], finding that acicular structures may be obtained in nickel–molybdenum gray cast irons in the as-cast condition, as long as the alloying elements were properly adjusted in relation to the cooling rate. In their work they used casting wall thicknesses ranging from 25 to 150 mm, to evaluate the effect of two molybdenum additions (0.1% and 0.5%) with varying nickel contents ranging from 1.0% to 5.0%. Fig. 3 illustrates their main findings for the effect of Ni and Mo additions on the transformation curve. From heats 2 to 4 there is an increasing Mo addition, revealing that with increments of this element there is a deeper accentuation of the bay contained in the TTT diagram. Furthermore, heats from 4 to 8 have constant levels of Mo with increasing levels of Ni. As it can be seen, nickel drops the temperatures that define the intercritical interval. Thanks to their study on the effect of Ni–Mo in the cooling process, Kashani and Boutorabi [11] managed to produce as-cast acicular ductile cast iron with a matrix composed of bainitic ferrite by means of alloying with 3.0%Ni and 0.66%Mo. Finally, the only study found as a DMS ductile iron achieved in an as-cast condition was reported by Nobuki et al. [32], where additions of Mn of 0.5% and 1.0% on castings with Ni > 3% produced a matrix structure with pearlite, bainite and ferrite on a casting wall thickness of 30 mm.

This paper studies the production of dual matrix structure as-cast ductile irons with low amounts of Mo, aiming at the development of high strength castings without incurring additional increases in production costs related with heat-treatments. It is acknowledged that previous studies investigated the effect of Ni–Mo and Ni–Mg additions on acicular DI [11,32]. However, those studies (i) performed heat treatments to allow higher ductility levels; (ii) used alloying quantities (Mo and Mg) higher than 0.5% that have a high impact on the final production cost; and (iii) did not consider that in a casting process different section sizes are involved, being the most common range being between 10 and 50 mm.

2. Experimental procedure

Eleven heats of cast iron were prepared in a commercial foundry using an induction furnace with a maximum capacity of 1200 kg, charged with 60% of cold rolled steel and 40% of pig iron. Once the materials were melted, and the respective carbon, silicon, nickel and molybdenum adjusted, the furnace was kept at a temperature of 1550 °C. The spheroidizing treatment was performed by means of the sandwich method, where once the ladle was preheated, 1.1% Fe–Si–Mg was covered by the reaction retarding material, reducing the Mg evaporation. When the spheroidizing treatment was ended, each melt was divided into 100 kg ladles. A further inoculation was performed in the ladles with 0.3% Fe–Si in order to avoid carbide formation.

After removal of the scum resulting from post-inoculation, castings were poured into the sand molds 1 min after the spheroidizing treatment (1380 °C < T < 1414 °C) in order to avoid any magnesium fading which could affect the nodule formation. Sand molds with Y block shape according to ASTM A 536 [41] were used to obtain tensile testing specimens (see Fig. 4a). Step sand molds were used to study the effect of wall thickness (and therefore cooling rate) on the microstructure of the material, following Kim et al. [42] (see Fig. 4b), having wall thicknesses of 10 mm, 30 mm and 50 mm.

The chemical compositions of the melts prior to the spheroidizing treatments, obtained by optical emission spectroscopy (OES) are given in Table 1. In order to evaluate the effect of Ni–Mo additions, the melts were divided in two different groups: in the first group, nickel was added between 1.0 < Ni% < and 7.0 and in the second group 0.2% molybdenum was added to the same levels of nickel used for the first group. The carbon equivalent (CE) was calculated in order to verify that all the produced melts had similar paths during the solidification process, finding that most of them are close to be eutectic. The CE is important since it determines if the DI is hyper, hypo or eutectic, which modifies the solidification process during eutectic solidification. However, since the aim of this study was to study the transformation of the matrix, the CE does not play an important role as the matrix transformation happens during the eutectoid transformation, when all austenite and graphite nodules are already formed. Furthermore the Mn content varies between 0.08 < Mn < 0.35. However manganese has an impact on the properties of ductile irons when it is added between 0.5 < Mn < 0.8, therefore the levels of Mn found in the analyzed melts have no effect on mechanical properties or the intercritical temperature range [4].

Optical (OM) and Scanning Electron Microscopy (SEM) were used for the microstructural characterization of the castings. Specimens were taken from the last solidification zone of each casting, found by numerical simulation using the software Solid-Cast® and shown as the highlighted yellow region in Fig. 4, for each mold shape. For the Y block, the last zone to solidify corresponds to the top of the block, since it is designed with that purpose. However, the last zone to solidify closest to the probes

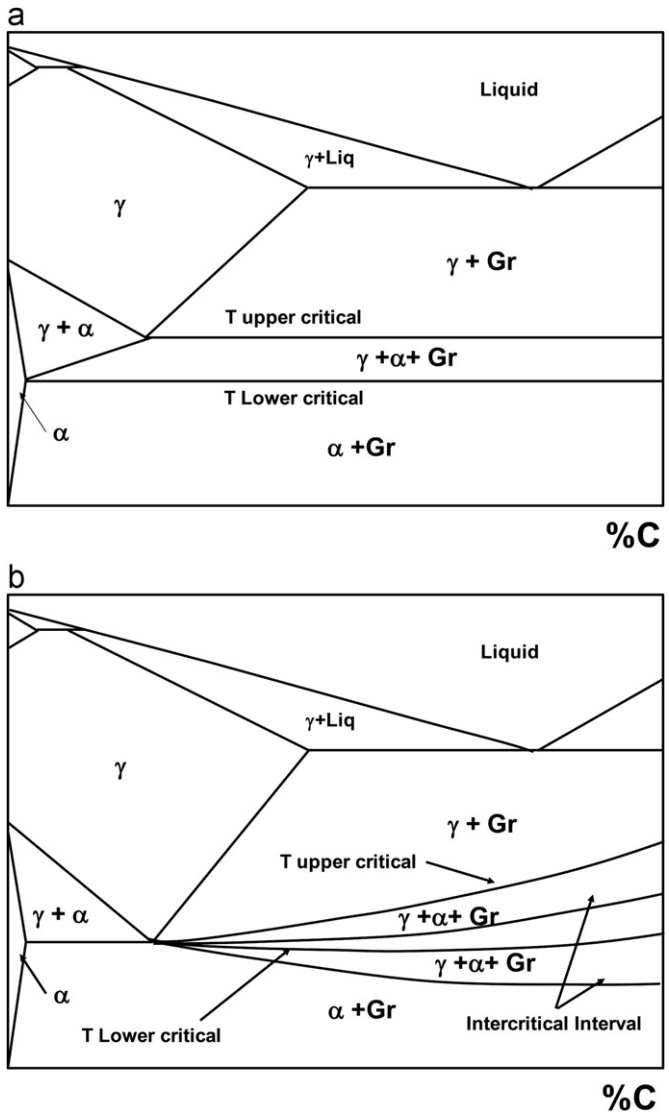

Fig. 2. Schematic representation of the Fe–C phase diagram[3] (a) at 2.5%Si; and (b) effect on the intercritical interval position of increasing amounts of Si (continuous line) and increasing amounts of Ni (dotted line).

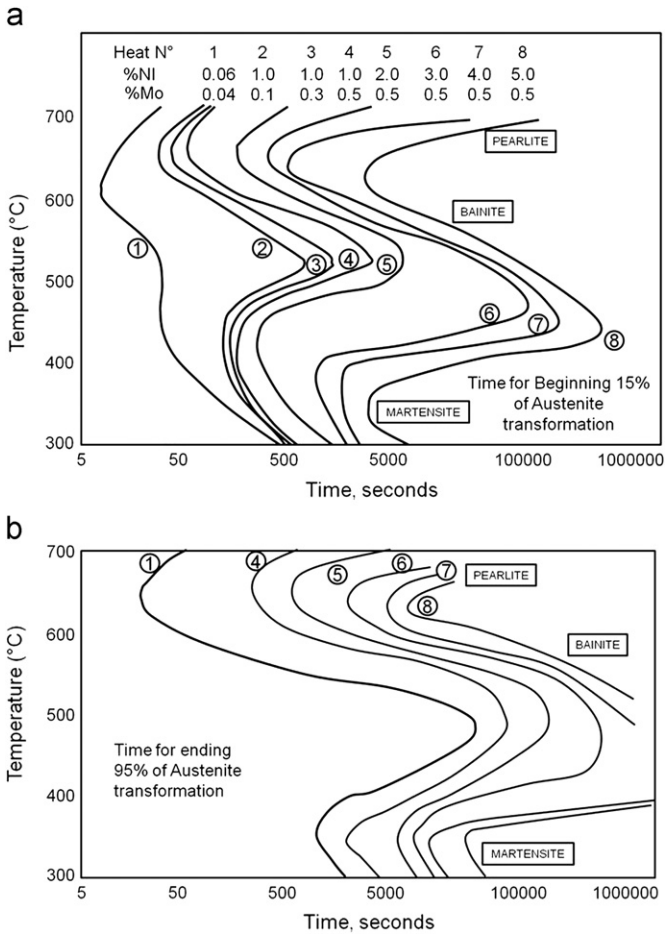

Fig. 3. Transformation curves for cast irons showing the effect of Ni–Mo on the times of (a) beginning and (b) ending of austenite transformation [40].

taken for mechanical testing is shown in Fig. 4(a), taking 6 min to complete solidification. As shown in Fig. 4(b), the step mold has two different highlighted zones due to the changes in thickness. The highlighted zones that correspond to the 50 and 30 mm thicknesses had a solidification time of 4.71 min, while the 10 mm zone took just 1.57 min. Conventional metallographic preparation of the specimens was followed and is described elsewhere [43]. With the purpose of distinguishing bainite from other microstructures, sodium metalsulfite with a concentration of 1% was used as chemical etching reagent. Nodule count, nodularity of graphite nodules, area fraction of ferrite, pearlite and acicular structures were analyzed via image analysis software.

X-ray diffraction analyses were carried out using an Xpert Pro® difractometer with CuKα radiation, using continuous scanning at $0.013^{\circ}\,s^{-1}$ over $2\theta = 30–150^{\circ}$, in order to identify the presence of retained austenite. Lattice parameters were calculated using Bragg's law to support the structures found by optical and scanning microscopy [44].

To characterize the castings produced and the effect of Ni–Mo additions on the final properties of the DI [41,45,46], tensile testing, Brinell and Vickers hardness testing were performed with the use of a Schenck Trebel universal testing machine, an Albert Gnehm hardness tester and a Wilson instruments micro-hardness tester, respectively. For Brinell hardness, a hardened steel indenter of 2.5 mm of diameter was used with an applied force of 187.5 kg.

3. Results and discussion

3.1. Microstructure

Fig. 5 shows representative microstructures obtained for the nickel DI group for a wall thickness of 30 mm (see Fig. 4). Results for the other two thicknesses studied (10 and 50 mm) showed similar microstructures to those presented in Fig. 5, and therefore are not shown. It is worth mentioning here that all the remaining results and discussions presented will be devoted to the 30 mm thickness samples, unless otherwise stated.

Fig. 5a–d shows the differences on the matrix distribution with increasing amounts of Ni (1%, 3%, 5% and 7%, correspondingly). Additions of Ni up to 5% showed an increase in the amount of pearlite, while its laminar space was reduced, getting fine pearlite (see Fig. 5f). For the casting with 7% Ni, bainite was obtained in a martensite matrix, while some ferrite surrounded the graphite nodules, as shown in Fig. 5d and e at higher magnification. From the study by Finn et al. [40], it is known that the effect of nickel additions to the castings is to cause a progressive downward displacement of the temperatures that limit the intercritical interval (see Fig. 2). Hence, with the same cooling rate but

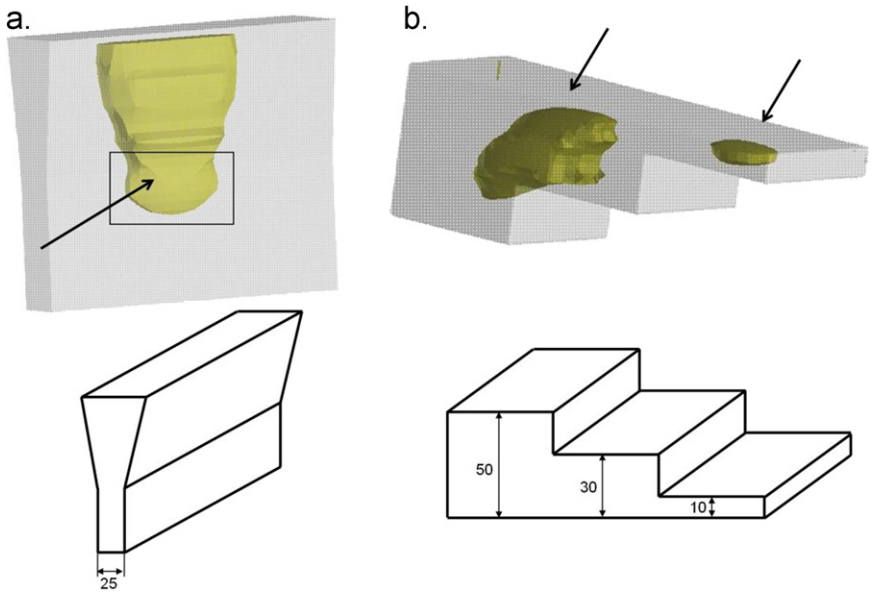

Fig. 4. Sand casting shapes used for the castings. (a) Y block mold casting used to obtain tensile samples. (b) Step casting used to evaluate the effect of wall thickness [42]. The yellow zones indicate the last zone to solidify in each sample. Measurements are in millimeter. (For interpretation of the references to color in this figure legend, the reader is referred to the web version of this article.)

Table 1
Chemical composition of DI iron samples produced, mass%.

Group	Sample (%)	Fe	C	Mn	P	S	Si	Ni	Cr	Cu	Mo	Mg	CE
	Base	93.55	3.76	0.35	0.01	0.01	2.26	0.00	0.00	0.018	0.00	0.05	4.51
Ni	1 Ni	92.74	3.34	0.08	0.00	0.00	2.83	0.97	0.00	0.10	0.00	0.02	4.29
	3 Ni	90.60	3.35	0.31	0.00	0.01	2.59	2.93	0.03	0.00	0.05	0.03	4.22
	5 Ni	87.83	3.85	0.22	0.01	0.01	2.64	5.22	0.02	0.05	0.00	0.05	4.72
	7 Ni	86.56	3.43	0.18	0.01	0.02	2.49	7.07	0.00	0.00	0.04	0.05	4.26
Ni–Mo	1 NiMo	91.75	3.56	0.37	0.02	0.02	2.89	0.95	0.03	0.06	0.19	0.05	4.52
	3 NiMo	90.25	3.52	0.21	0.00	0.01	2.52	3.02	0.03	0.00	0.29	0.04	4.36
	5 NiMo	87.13	4.04	0.23	0.02	0.02	2.83	5.31	0.03	0.05	0.19	0.05	4.99
	7 NiMo	86.73	3.03	0.24	0.01	0.02	2.62	6.86	0.08	0.02	0.30	0.03	3.90

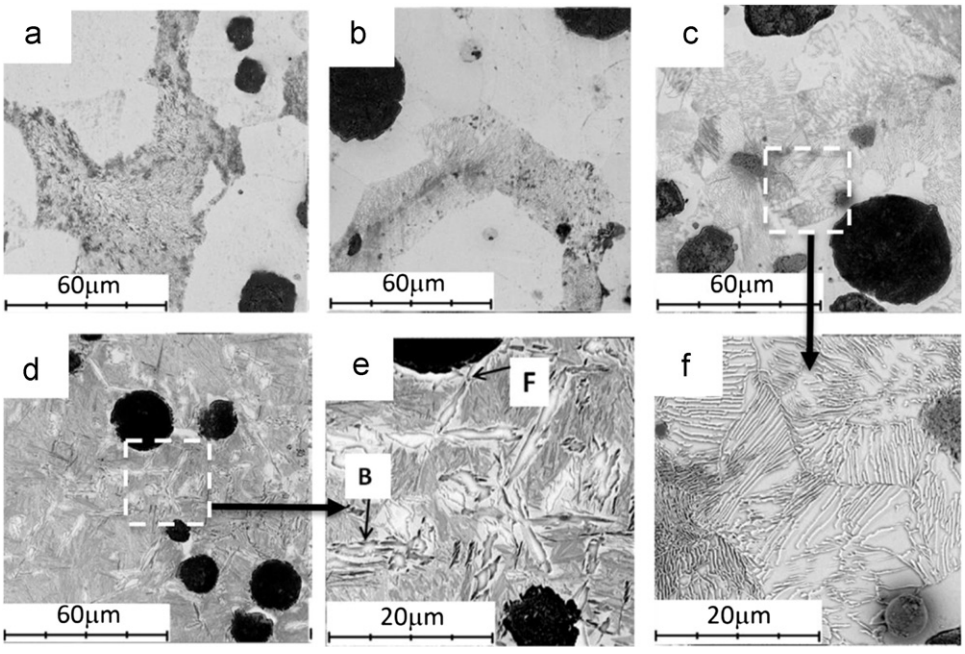

Fig. 5. Evolution of ductile iron microstructures with addition of nickel: (a) 1% Ni; (b) 3% Ni; (c) 5% Ni; (d) 7% Ni; (e) 7% Ni at higher magnification, indicating ferrite (F) and bainite (B) and (f) 5% Ni at higher magnification showing Pearlite.

increasing levels of Ni it is possible to obtain acicular structures, as confirmed by the obtained results.

Matrix characteristics for the 30 mm wall thickness castings are shown in Table 2, these results have the same tendency of the remaining section sizes with an increase of nodule count as the thickness is reduced, as expected. The graphite nodularity (*gn*) of the castings varies in a range between $69\% < gn < 78\%$, suggesting that the addition of Ni is not affecting the nodulization treatment. Since the nodule characterization was performed by means of image analysis software, it is important to consider that a *gn* greater than 65% is considered optimum to classify the casting as ductile iron [47]. It can also be noted that, as Table 2 and the micrographs of Fig. 5 show, with an increase of nickel there is an increase in the amount of pearlite, with a consequent decrease in the amount of ferrite. For sample 7 Ni, most of the matrix is composed of acicular structures, leaving only ~1.2% of ferrite. This amount of ferrite is not enough to classify the casting as DMS, since the lowest reported amount of ferrite for a DMS is ~5% [1,3,18,19,25–27,32].

Fig. 6 shows the microstructures of the Ni–Mo DI group. In comparison with Ni additions, pearlite from sample 1 NiMo (Fig. 6a and e) resembles the final pearlite structure of sample 4Ni (Fig. 5d), which suggests that Mo additions promote finer pearlite structures. Additionally, in sample 3 NiMo (Fig. 6b and f) there is a mixture of acicular structures with pearlite. In samples 5 NiMo (Fig. 6c and g) and 7 NiMo (Fig. 6d and h) there is a transformation inside the casting mold from austenite to martensite and bainite structures with the presence of ferrite, therefore a DMS ductile iron was achieved. In order to obtain these transformations within the sand mold, there must be a change in the transformation curve due to the alloying elements used. Fig. 3 shows how the transformation curves change with the addition of Ni and Ni–Mo, according to the study of Flinn et al. [40], where heats from 1 to 3 show that with increasing amount of Mo there is an accentuation on the bay formed between 500 °C and 600 °C, which extends the time for a possible formation of finer pearlite and acicular structures. On the other hand, incremental additions of Ni (heats 4–8) produce a drop in the temperatures defining the intercritical interval. Therefore, with NiMo additions to the casting there is a shift to the right on the curve and a decrease in the temperature for the beginning of matrix transformation, allowing different microstructures with the same cooling rate. It is important to note that even with the presence of acicular structures there is still ferrite present in the metallic matrix, which will contribute to maintain some of the characteristic ductility of DI castings.

Table 3 shows the matrix characteristics found for the wall thickness of 30 mm for the Ni–Mo group castings. With additions of NiMo the graphite nodularity (*gn*) varies in the range between $68\% < gn < 77\%$, which suggests that the addition of NiMo does not affect the graphite nodule shape in the DI castings. Comparing with data from Table 2, on additions of molybdenum there is an increase in the area fraction of pearlite in the matrix. For sample 3 NiMo the image segmentation to differentiate between pearlite and acicular structures presented difficulties, therefore the area fraction of acicular structures reported for this sample also includes pearlite. It is important to note that even though the area fraction of ferrite (*af*) decreases with increasing nickel, the addition of Mo makes possible a range between $7\% < af < 63\%$ which is in close agreement with the reported values of DMS after heat treatments for DI castings [3,19,25].

X-ray diffraction (XRD) patterns of the melts were analyzed in order to confirm the nature of the obtained acicular structures. The X-ray patterns from the 5 Ni and 5 NiMo castings are shown in Fig. 7 (representative of the remaining difractograms), where

Table 2
Results of metallographic measurement for nickel alloy (average values).

Matrix characteristic	Base	±	1 Ni	±	3 Ni	±	5 Ni	±	7 Ni	±
Graphite nodularity (%)	68.94	1.70	72.33	0.88	77.00	0.88	70.40	1.29	78.20	1.32
Area fraction of graphite (%)	11.81	1.38	15.00	0.82	15.00	1.42	15.00	0.89	13.00	1.10
Nodule count per unit area (mm^{-2})	216.18	2.15	216.00	1.15	215.00	2.76	193.00	3.86	320.00	4.03
Area fraction of ferrite (%)	71.08	2.33	67.70	1.11	50.10	2.28	9.40	1.43	1.20	1.21
Area fraction of pearlite (%)	17.11	1.62	17.30	0.15	34.90	2.30	75.60	2.75	–	–
Area fraction of acicular structures (%)	–	–	–	–	–	–	–	–	85.80	1.06

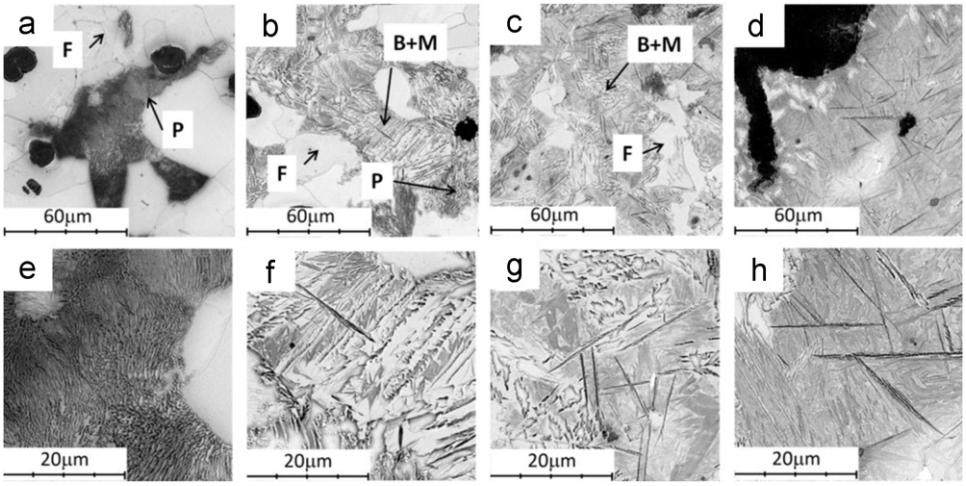

Fig. 6. Evolution of ductile iron microstructures with addition of nickel and molybdenum: (a) 1% NiMo showing ferrite (F) and pearlite (P); (b) 3% NiMo showing ferrite (F), pearlite (P), bainite (B) and martensite (M); (c) 5% NiMo showing ferrite (F), bainite (B) and martensite (M); (d) 7% NiMo showing acicular structures. (e) 1% NiMo at higher magnification; (f) 3% NiMo at higher magnification; (g) 5% NiMo at higher magnification; and (h) 7% NiMo at higher magnification.

Table 3
Results of metallographic measurement for Ni–Mo alloy (average values).

Matrix characteristic	Base	±	1 NiMo	±	3 NiMo	±	5 NiMo	±	7 NiMo	±
Graphite nodularity (%)	68.94	1.70	75.70	2.13	77.00	2.00	73.40	2.42	67.40	2.38
Area fraction of graphite (%)	11.81	1.38	14.10	1.31	11.00	1.49	15.70	1.53	12.90	1.45
Nodule count per unit area (mm^{-2})	216.18	2.15	296.00	3.86	215.00	4.76	258.00	3.52	261.00	4.05
Area fraction of ferrite (%)	71.08	2.33	63.00	2.15	34.70	2.98	6.70	1.33	7.60	1.25
Area fraction of pearlite (%)	17.11	1.62	22.90	1.10	–	–	–	–	–	–
Area fraction of acicular structres (%)	–	–	–	–	54.30	1.59	77.60	1.32	79.50	1.92

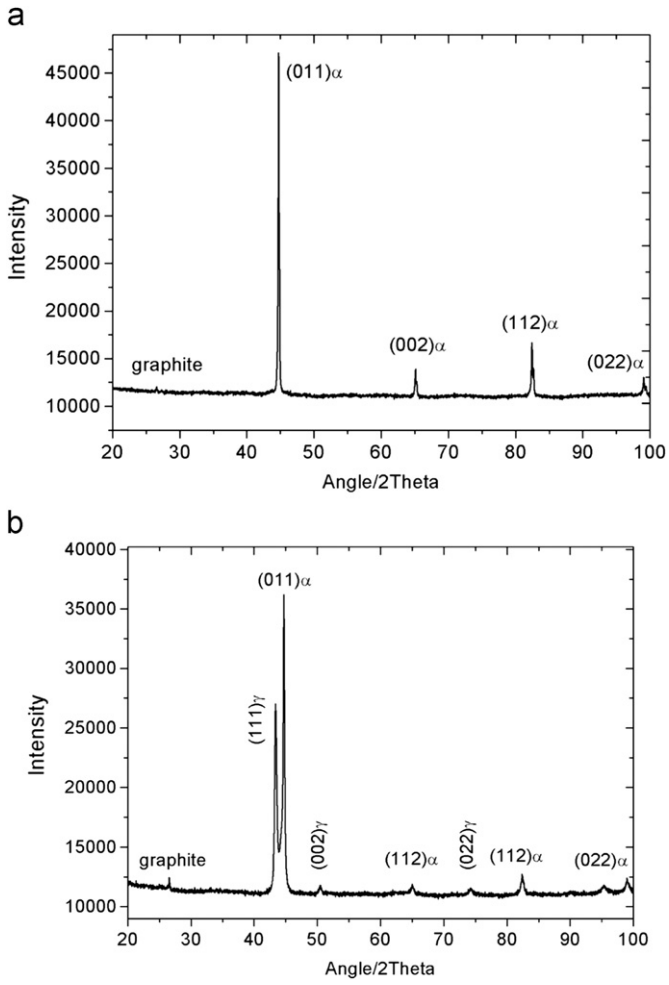

Fig. 7. X-ray diffraction experiments: (a) sample 5 Ni and (b) sample 5 NiMo.

the (111), (002) and (113) planes of fcc austenite and (011), (002), (112) and (022) planes of bcc ferrite are shown [48,49]. As shown in Fig. 7(a), the Ni group DI castings only showed diffraction peaks that correspond to ferrite, which is in close agreement with the results from Fig. 5, where the microstructure is mainly composed of ferrite and pearlite. However, when acicular structures like bainite are generated during the solidification process, retained austenite tends to appear in the matrix. During the transformation of austenite to bainite, there is a point where all of the possible nucleation sites for bainite are created and as a result some austenite remains in the matrix, making it possible to detect it by XRD [11,48]. As a consequence, the samples that had precipitation of bainite showed austenite diffraction peaks as shown in Fig. 7(b). Additionally, each pattern analyzed showed a diffraction peak at 26.5°, corresponding to the graphite present in the DI castings [13]. Lattice parameters of ferrite and austenite were calculated and are shown in Table 4. The lattice parameters

Table 4
Summary of the X-ray diffraction analysis.

Sample	a_γ		a_α	
	Ni	NiMo	Ni	NiMo
1	–	–	2.8598	2.8601
3	–	3.6189	2.8626	2.8618
5	–	3.6107	2.8597	2.8638
7	3.5974	3.5997	2.8645	2.8634

found for austenite in the different melts are in close agreement with those reported by other authors, which confirms the presence of austenite, as shown by the diffraction peaks found in their studies [40,48,49]. However, the lattice parameter for "ferrite" is difficult to interpret as it reflects that of both martensite and bainitic ferrite, since they are strained versions of the initial structure of ferrite. Nonetheless, the results in Table 4 are in close agreement with the lattice parameters reported for tempering and austempering of DI castings by other authors, where the mean values (a_α) for bainitic ferrite can be found between $2.861 < a_\alpha < 2.867$ [40,48,49]. Hence acicular structures like bainite and martensite were correctly identified with the performed microstructural analysis.

Having already found DMS ductile iron thanks to the NiMo additions, it is important to look over the conditions under which acicular structures and ferrite are obtained in an as-cast state. In a casting process there are usually variations in the wall thicknesses of the products, therefore it is common to have different cooling rates on a single element to be casted. Hence, it is important to corroborate if the desired DMS is going to be obtained for typical or representative cooling rates found on the manufacturing process. Fig. 3 shows the isothermal transformation curves for different amounts of Ni and Mo at the beginning and ending of the austenite transformation, according to the study of Flinn et al. [40]. If the cooling process has a higher or lower cooling rate the final matrix microstructure would change. Accordingly, the formation of bainite during continuous cooling requires a cooling rate fast enough to avoid the transformation of austenite into pearlite. Additionally, if the cooling rate is too fast, the bainite transformation will be suppressed and martensite would appear. This possible change of matrix structure depending on the cooling rate was evaluated with the use of the step molds with different wall thicknesses (10, 30 and 50 mm) representative of the most common commercial thicknesses used on DI castings (see Fig. 4). Fig. 8 shows the matrix microstructure distribution for these wall thicknesses. It is worth mentioning that in this figure the amounts of ferrite and graphite present on the matrix are not shown. Nonetheless, the mean value of graphite content is ~13% with the remaining percentage corresponding to the ferrite present in the matrix. It can be seen that for a fixed amount of NiMo, all of the wall thicknesses exhibit similar quantities of the microstructures in the metal matrix, which suggests that even with varying wall thicknesses (cooling rates) it is possible to achieve DMS as-cast ductile iron. Similar microstructures were

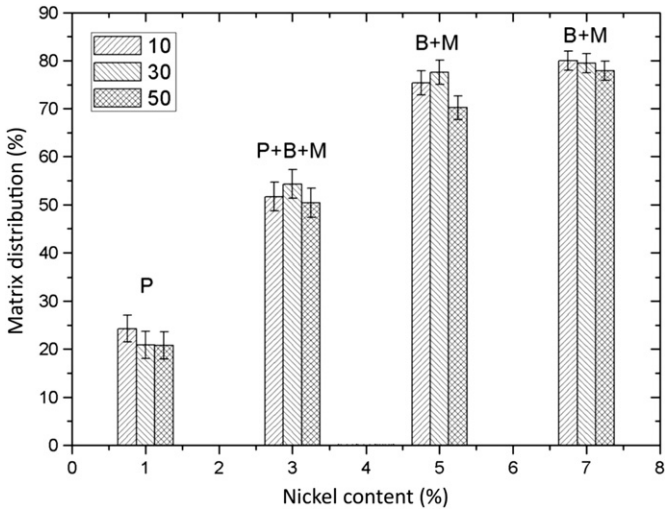

Fig. 8. Effect of Ni–Mo content and casting wall thickness on matrix distribution. On top of each set of bars are given the structures present: pearlite (P), bainite (B) and martensite (M).

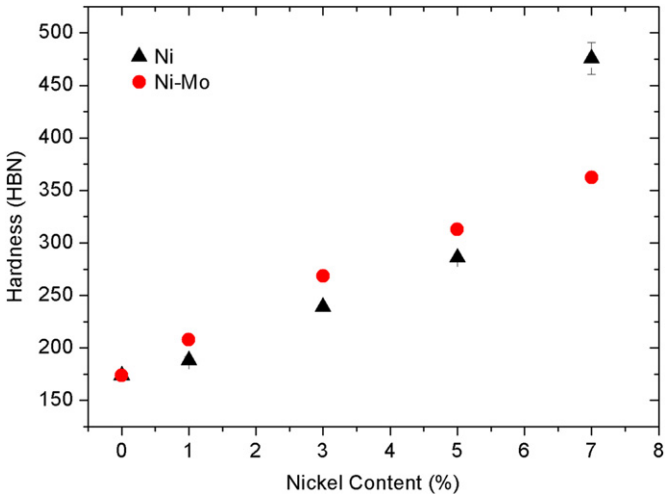

Fig. 9. Brinell hardness for the Ni–Mo castings.

achieved due to low changes in the evaluated wall thicknesses (maximum difference of 40 mm). From literature it was found that changes in the microstructure are experienced with a difference of wall thickness of 50 mm according to the Ni additions [40]. In spite of that, cooling rate must be carefully considered when the material is expected to have certain amount of ductility, as decreasing wall thickness will increase cooling rate and as a consequence there will be a reduction in the final ferrite area fraction, with the subsequent reduction in ductility of the DI casting.

3.2. Mechanical properties

Fig. 9 shows the Brinell hardness values obtained for the Ni and NiMo casting groups. In general, increasing levels of Nickel produce higher values of hardness, due to the achieved microstructure. The Ni group showed a tendency of decreasing the area fraction of ferrite (softer phase) while increasing the amount of finer pearlite (harder phase). For the 7 Ni sample there is an increase of ~200 HBN in comparison to 5Ni due to the appearance of bainite and martensite in the structure.

Addition of Mo results in a slight increase in hardness in comparison to the Ni group up to 5% Ni. The raise in sample 1 NiMo can be explained by the precipitation of finer pearlite. While the other NiMo samples show higher hardness values due to the precipitation of acicular structures (bainite and martensite). The 7 NiMo sample shows a lower hardness in comparison to the 7 Ni sample due to the reduced presence of ferrite on the matrix of the 7 Ni sample.

Table 5 shows the values for Vickers microhardness of the different matrix structures found in the castings, getting results consistent with previous studies [32]. As a general rule, harder microstructures produce higher levels of strength on the material. In spite of that, harder phases also contribute to reduction in the ductility of DI. Figs. 10 and 11 show the effect of Ni and Ni–Mo additions on the tensile strength and ductility of the DI castings, respectively. As Ni content increases, higher levels of tensile strength can be achieved. For the Ni group, the increase of strength is given by the evolution of pearlite and change of matrix distribution. For instance, sample 5 Ni has the larger area fraction of pearlite in all of the Ni group, therefore exhibiting higher levels of strength. Nonetheless, having a largest area fraction of pearlite induces a decrease in the amount of ferrite. As a consequence, the ductility found for the 5Ni sample is the lowest of the Ni group when acicular structures are not present in the microstructure. Since acicular microstructures produce higher levels of strength, for the Ni group the 7 Ni sample showed the highest tensile strength with the lowest elongation. When molybdenum is added, the DMS shows an increase of ~25% in the tensile strength when compared to the Ni group. This enhancement in strength is possible because of the presence of acicular structures in the metal matrix. Even so, the NiMo group has lower ductility since acicular structures are more brittle than pearlite. Additionally, sample 7 Ni shows higher strength than sample 7 NiMo mainly due to two factors: (i) 7 Ni sample has less ferrite in the metal matrix, which provides the DI with a higher value of strength; and (ii) 7 NiMo sample has lower graphite nodularity, reducing the expected strength. Lower nodularity can reduce the maximum tensile strength of ductile irons; however, a change of 10% in nodularity is not significant enough to reduce the elongations, hence the similar values for this characteristic in both samples are analyzed [6].

An important outcome from the present work is that the strength and ductility of the DMS as-cast ductile iron have similar values of mechanical properties as those achieved for Austempered Ductile Iron (ADI) [7,9,36]. Therefore, the use of NiMo enables the production of DI with improved properties without further heat-treating processes. The combination of strength and elongation found for 3 NiMo and 5 NiMo samples reflect the mean properties of the reported DMS structures [1,3,18,19,25–27]. Therefore, the extra cost due to heat treatment process can be avoided.

4. Concluding remarks

Dual matrix structure as-cast ductile irons with nickel in concentrations up to 7% and low amounts of molybdenum were produced and characterized from the perspective of microstructure and mechanical properties, for castings with wall thicknesses ranging from 10 to 50 mm. It was found that with additions of 0.2% Mo and without further heat treatments it is possible to obtain acicular structures (bainite and martensite) with the presence of ferrite, achieving mechanical properties similar to those of ductile irons after heat treatment processes such as tempering and austempering. Additionally, it was found that with a fixed amount of Ni–Mo, similar microstructures could be achieved for the most common wall thicknesses used for ductile

Table 5
Vickers hardness of each microstructure (average values).

Sample	Ferrite				Pearlite				Acicular structures			
	Ni	±	Ni–Mo	±	Ni	±	Ni–Mo	±	Ni	±	Ni–Mo	±
0	200.60	0.96	200.60	0.48	292.83	0.96	292.83	0.48	–	–	–	–
1	167.60	0.99	171.90	1.41	296.45	2.84	309.55	3.67	–	–	–	–
3	178.85	2.47	179.95	1.48	319.95	0.78	370.25	1.63	–	–	452.70	3.90
5	182.75	3.39	190.95	4.30	363.35	2.45	–	–	–	–	600.3	4.30
7	–	–	–	–	–	–	–	–	664.50	2.60	624.13	1.20

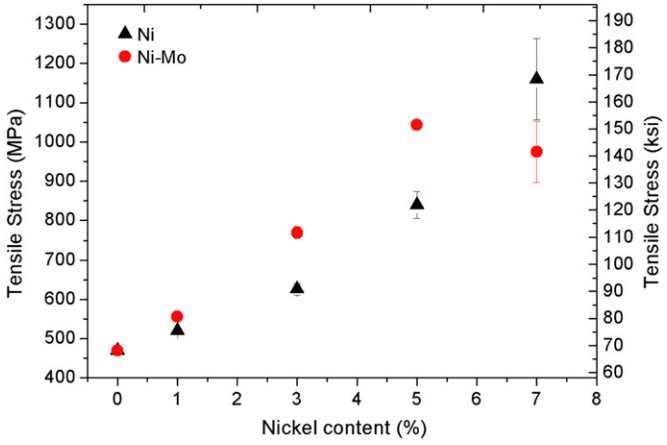

Fig. 10. Tensile strengths for the Ni–Mo castings.

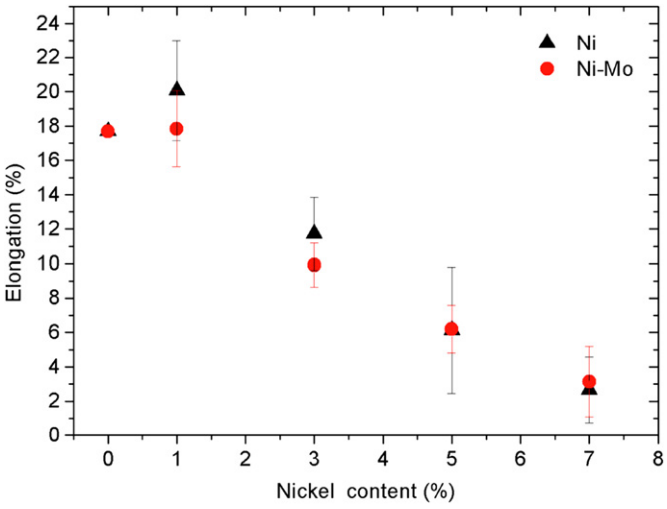

Fig. 11. Elongation for the Ni–Mo castings.

iron castings. Nonetheless, wall thickness should be carefully considered, as ductility can be reduced considerably for thinner wall thicknesses, as fast cooling rates will reduce the amounts of ferrite on the matrix.

Acknowledgments

The authors would like to express their gratitude to the foundry Furima S.A.S, Medellín, Colombia, for providing the materials used in this study. It is also important to acknowledge the economic support for this study provided by the Administrative Department of Science, Technology and Innovation, Colciencias (Colombia) by Contract no. 525-09.

References

[1] K. Kocatepe, M. Cerah, M. Erdogan, J. Mater. Process. Technol. 178 (2006) 44–51.
[2] M. Hafiz, J. Mater. Sci. 36 (2001) 1293–1300.
[3] A. Basso, J. Sikora, Int. J. Metalcast. 6 (2012) 7–14.
[4] A.F.M.S.S. Inc., AFS Ductile Iron Handbook,, AFS, 1993.
[5] A.S.M. Handbook, vol. 1, 2005.
[6] S.C. Murcia, Estudio del efecto de las variables de proceso sobre la calidad final en fundiciones de hierro nodular, Production Engineering, Eafit University, 2010.
[7] A. Refaey, N. Fatahalla, J. Mater. Sci. 38 (2003) 351–362.
[8] S.C. Lee, C.H. Hsu, H.P. Feng, C.C. Chang, Metall. Mater. Trans. A 29 (1998) 2511–2521.
[9] M. Cerah, K. Kocatepe, M. Erdogan, J. Mater. Sci. 40 (2005) 3453–3459.
[10] M. Ferry, W. Xu, Mater. Char. 53 (2004) 43–49.
[11] S.M.M. Kashani, S. Boutorabi, J. Iron Steel Res., Int. 16 (2009) 23–28.
[12] M. Martinez Celis, N. Valle, J. Lacaze, I. Thorbjornsson, B. Johannesson, J. Thorgrimsson, Int. J. Cast Met. Res. 24 (2011) 76–82.
[13] J.P. Altuve, M. Marrero, W. Meléndez, M. Martínez, J. González, Comparación de dos técnicas instrumentales (DRX y Raman), en el estudio deparámetros cristalográficos de manifestaciones grafitosas, IX Congreso Geológico Venezolano.
[14] J. Yang, S.K. Putatunda, Mater. Des. 25 (2004) 219–230.
[15] S. Zahiri, E. Pereloma, C. Davies, Mater. Sci. Technol. 17 (2001) 1563–1568.
[16] M.N. Ahmadabadi, R. Shamloo, J. Phase Equilibria22 (2001) 194–198.
[17] Z. El-Baradie, M. Ibrahim, I. El-Sisy, A.Abd. El-Hakeem, Mater. Sci. 40 (2004) 523–528.
[18] A. Basso, R. Martínez, J. Sikora, Mater. Sci. Technol. 23 (2007) 1321–1326.
[19] M. Erdogan, M. Cerah, K. Kocatepe, Int. J. Cast Met. Res. 19 (2006) 248–253.
[20] R.K. Panda, J.P. Dhal, S.C. Mishra, S. Sen, International J. Curr. Res. Rev. 4 (2012) 16–21.
[21] S.K. Putatunda, Mater. Sci. Eng.: A 315 (2001) 70–80.
[22] U. Batra, S. Ray, S. Prabhakar, J. Mater. Eng. Perform. 14 (2005) 574–581.
[23] K. Laneri, J. Desimoni, R. Mercader, R. Gregorutti, J. Sarutti, Metall. Mater. Trans. A 32 (2001) 51–58.
[24] M.A. Yescas, H. Bhadeshia, Mater. Sci. Eng.: A 333 (2002) 60–66.
[25] M. Erdogan, V. Kilicli, B. Demir, J. Mater. Sci. 44 (2009) 1394–1403.
[26] V. Kilicli, M. Erdogan, Mater. Sci. Technol. 22 (2006) 919–928.
[27] A.M. Rashidi, M. Moshrefi-Torbati, Mater. Lett. 45 (2000) 203–207.
[28] M. Nili Ahmadabadi, Metall. Mater. Trans. A 29 (1998) 2297–2306.
[29] B. Bosnjak, V. Asanovic, B. Radulovic, K. Pop-Tonev, J. Mater. Eng. Perform. 10 (2001) 203–211.
[30] H.N. El-Din, A. Nofal, K. Ibrahim, A. Ramadan, Int. J. Cast Met. Res. 19 (2006) 137–150.
[31] K. Ibrahim, Int. J. Cast Met. Res. 18 (2005) 309–314.
[32] T. Nobuki, M. Hatate, T. Shiota, Int. J. Cast Met. Res. 21 (1) (2008) 31–38.
[33] M. Ramadan, A. Nofal, I. Elmahalawi, R. Abdel-Karim, Int. J. Cast Met. Res. 19 (2006) 151–155.
[34] U. Batra, S. Ray, S. Prabhakar, J. Mater. Eng. Perform. 13 (2004) 64–68.
[35] M. Nili Ahmadabadi, H. Ghasemi, M. Osia, Wear 231 (1999) 293–300.
[36] O. Erić, M. Jovanović, D. Rajnović, S. Zec, Mater. Des. 27 (2006) 617–622.
[37] P. Shelton, A. Bonner, J. Mater. Process. Technol. 173 (2006) 269–274.
[38] Y.C. Peng, H.J. Jin, J.H. Liu, G.L. Li, Mater. Sci. Eng.: A 529 (2011) 321–325.
[39] N. Fatahalla, A. AbuElEzz, M. Semeida, Mater. Sci. Eng.: A 504 (2009) 81–89.
[40] R. Flinn, M. Cohen, J. Chipman, Trans. Am. Soc. Met. 30 (1942) 1255–1283.
[41] ASTM, Standard Specificaction for Ductile Iron Castings, American Society for Testing and Materials, A536-84.
[42] A. Kim, S.L. Cockcroft, A.M. Omrana, J. Alloys Compd. 476 (2009) 728–732.
[43] ASTM, Standard Guide for Preparation of Metallographic Specimens, E3-O1., ASTM International.
[44] D.R. Askeland, Ciencia e Ingeniería de los Materiales, Thomson-Paraninfo, 2001.
[45] ASTM, Standard Test Method for Brinell Hardness of Metallic Materials, E10-12, ASTM International.
[46] ASTM, Standard Test Method for Knoop and Vickers Hardness of Materials, E384-11e1, ASTM International.
[47] B. Imasogie, U. Wendt, J. Miner. Mater. Charact. Eng. 3 (2004) 1–12.
[48] M.J. Peet, Transformation and Tempering of Low-temperature bainite, Doctor of Philosophy, University of Cambridge, 2010.
[49] A. Saha Podder, H. Bhadeshia, Mater. Sci. Eng.: A 527 (2010) 2121–2128.